Implementation of large-scale average geostrophic wind shear in WAsP12.1

Floors, Rogier Ralph; Troen, Ib; Kelly, Mark C.

Publication date:
2018

Document Version
Publisher's PDF, also known as Version of record

Implementation of large-scale average geostrophic wind shear in WAsP 12.1

Department of Wind Energy E Report 2018

Rogier Floors, Ib Troen and Mark Kelly

DTU Wind Energy Report-E-0169

June 2018

DTU Wind Energy
Department of Wind Energy

Authors: Rogier Floors, Ib Troen, Mark Kelly
Title: Implementation of large-scale average geostrophic wind shear in WAsP12.1
Department: DTU Wind Energy

DTU Wind Energy-E-Report-0169(EN)
June 12, 2018

ISSN:
ISBN:
978-87-93549-37-1

Abstract (max. 2000 char)

The vertical extrapolation model described in the European Wind Atlas Troen and Petersen (1989) is modified to take into account large-scale average geostrophic wind shear to describe the effect of horizontal temperature gradients on the geostrophic wind. The method is implemented by extracting the average geostrophic wind shear from Climate Forecast System Reanalysis (CFSR) data and the values of nearest grid point are automatically used in the WAsP 12.1 user interface to provide better AEP predictions.

Contract no:

Project no:

Sponsorship:
Internal funding

Cover: External cover

Pages: 10
Tables: 1
Figures: 2
References: 14

Technical University of Denmark
Frederiksborgvej 399
4000 Roskilde
Denmark
Tel. +4546775085
www.vindenergi.dtu.dk

Contents

1 Theory

1.1 Extrapolation using the geostrophic drag law

The extrapolation of wind in the Wind Atlas Analysis and Application Program (WAsP) utilizes Monin-Obukhov similarity theory and the geostrophic drag law (Troen and Petersen, 1989; Blackadar and Tennekes, 1968). Because the long-term mean profile is generally close to neutral, it models the effect of atmospheric stability as perturbations to a neutral state (Troen and Petersen, 1989). In neutral conditions the geostrophic drag law is given by

$$G = \frac{u_*}{\kappa}\sqrt{\left(\ln\frac{u_*}{fz_0} - A_0\right)^2 + B_0^2} \tag{1}$$

where G is the geostrophic wind speed, f is the Coriolis parameter, κ is the von Kármán constant (≈ 0.4), z_0 is the mesoscale roughness length and A_0 and B_0 are empirical constants. In WAsP, values of $A_0 = 1.8$ and $B_0 = 4.5$ have been adopted, which are in good correspondence with an extensive survey of these constants at the mid-latitudes Hess and Garratt (2002). The stability-induced perturbation of the friction velocity u_* from its neutral value is derived via a first-order expansion due to surface-layer sensible heat flux H via Eq. 1 (Troen and Petersen, 1989; Kelly et al., 2014):

$$\left[1 + \left(\ln \mathrm{Ro} + \ln\frac{u_*}{G} - A\right)\left(\frac{u_*}{\kappa G}\right)^2\right]\frac{du_*}{u_*} = \frac{cg}{fT_0 c_p \rho G^2}dH, \tag{2}$$

where $\mathrm{Ro} \equiv G/fz_0$ is the surface Rossby number, g/T_0 is the buoyancy parameter, and c_p is the specific heat of air. The dependence of geostrophic wind upon stability is taken into account through the factor

$$c = B\frac{dB}{d\mu} - \left(\ln \mathrm{Ro} + \ln\frac{u_*}{G} - A\right)\frac{dA}{d\mu}, \tag{3}$$

where the Monin-Kazanski stability parameter $\mu \equiv \kappa u_*/fL$. In (2) the term in square brackets and c are assumed constant in Troen and Petersen (1989), where a value of 2.5 was adopted. In WAsP11 and WAsP10, the value was chosen to be 1.65, while WAsP12 and above this expression is solved iteratively. Note that Eq. 2 is equal to Eq. 8.8 of the EWA, and is used to compute the offset from the neutral value of u_*; this is done by using both offset and root-mean-square of the sensible heat flux, H_{off} and H_{rms}, respectively. The EWA also introduced the concept of a reversal height, z_m, which is equal to the height where first-order effects of surface heat flux modulations vanish and where there is a minimum in wind speed variance. The derivation of the reversal height is given in Kelly and Troen (2016) and results in

$$\left[1 + \left(\ln \mathrm{Ro} + \ln\frac{u_*}{G} - A\right)\left(\frac{u_*}{\kappa G}\right)^2\right]\frac{z_m/z_0}{\ln(z_m/z_0)} = \frac{c\mathrm{Ro}}{ak}\left(\frac{u_*}{G}\right)^3, \tag{4}$$

where a is the slope of the dimensionless wind shear in stable conditions, $a = 4.7$ (Businger et al., 1971). This reversal height is equal to the height where the Weibull k parameter reaches its maximum (Kelly et al., 2014; Troen and Petersen, 1989).The geostrophic drag coefficient can be estimated using Eq. 1, but is in the EWA approximated by using the simplified geostrophic drag law Jensen (1978) and Eq. 4 is approximated with a power law that simplifies to

$$z_m = \alpha z_0 \mathrm{Ro}^{\beta}, \tag{5}$$

where the constants $\alpha = 0.002$ and $\beta = 0.9$. In WAsP 12 and above, (4) is solved iteratively without approximation.

1.2 Geostrophic wind shear

The stability dependence of A and B is accounted for in Eq. 2, but there is also a strong dependence of these constants on baroclinicity, i.e. the effect of varying geostrophic wind

with height (geostrophic wind shear, Arya and Wyngaard (1975); Arya (1978); Floors et al. (2015)). The effect of geostrophic wind shear on the constants of the geostrophic drag law can be taken into account by decomposing into a barotropic and a baroclinic part:

$$A_0 = A + A' = A + M_0 \cos(\beta - \delta - \theta), \tag{6}$$

$$B_0 = B + B' = B + M_0 \sin(\beta - \delta - \theta), \tag{7}$$

where β is the direction of the geostrophic wind shear, δ is an effective turning of the thermal wind direction ($\approx$ 35–45°, Arya (1978)), and θ is the wind direction. The dimensionless geostrophic shear magnitude is defined

$$M_0 = m\kappa \frac{h}{u_*} \frac{\partial |\mathbf{U}_g|}{\partial z}, \tag{8}$$

where m is a coefficient related to the shape of the geostrophic wind profile up to the boundary layer height $h = cu_{*0}/f$ (Arya and Wyngaard, 1975); for boundary-layer depth we adopt $c = 0.165$, which is consistent with the h that is assumed within the limiting of the stability-induced correction factors (Kelly and Troen, 2016).

In case of a constant geostrophic wind shear with height, $m = 1/2$, and with linearly decreasing geostrophic wind shear with height, $m = 1/3$ (Arya and Wyngaard, 1975). The geostrophic wind shear vector over a specified layer with thickness z can also be expressed in terms of horizontal gradients of the geopotential, Φ, at a level of constant pressure. This vector is commonly referred to as the thermal wind vector, where

$$U_T = -\frac{1}{f} \frac{\partial}{\partial y} (\Phi_z - \Phi_0) \tag{9}$$

$$V_T = \frac{1}{f} \frac{\partial}{\partial x} (\Phi_z - \Phi_0) \tag{10}$$

are the components of this vector in a geographical coordinate system (positive x directed eastward, e.g. Holton and Hakim, 2004); here Φ_z and Φ_0 are the geopotential at the top and bottom of a layer, respectively. The thermal wind vector is parallel to the isotherms with the cold air to the left and can therefore be roughly estimated from weather maps with long term mean temperatures at a certain pressure level. For example, when the annual mean temperature is decreasing towards the North, this results in a geostrophic wind that is increasing with height for westerlies and decreasing with height with for easterlies. This effect is illustrated in Fig. 5 of Floors et al. (2015) for sites in western Europe, where geostrophic winds from the east tend to decrease in magnitude with height, whereas westerly geostrophic winds show an increasing magnitude with height.

1.3 Implementation in WAsP

In this section we describe the implementation of a correction for the climatological impact of average geostrophic wind shear on the wind profile model within WAsP. WAsP is a combination of several physical models, which together can extrapolate wind statistics in both the vertical and horizontal directions. For applied sector-wise use of Eqs. 6–7, we assume that the long-term average geostrophic wind shear vector is independent of the surface wind direction, i.e. M_0 and β do not depend on which directional sector we consider near the surface in WAsP. Then we can calculate the geostrophic drag law constants for each sector i as

$$A_{0,i} = A_0 + A'_i = A_0 + M_0 \cos(\beta - \delta - \theta_i) \tag{11}$$

$$B_{0,i} = B_0 + B'_i = B_0 + M_0 \sin(\beta - \delta - \theta_i), \tag{12}$$

where $\beta = \arctan(V_T/U_T)$, $\theta_i = \arctan(V_i/U_i)$ and $\delta = 35°$. M_0 and β can be computed from numerical weather prediction models, as long as the geopotential is available for a given pressure level. For application in WAsP 12.1, they are estimated from large-scale reanalysis

data. The Climate Forecast System Reanalysis (CFSR) global reanalysis dataset version 2 (Saha et al., 2014), with a 0.5 degree (lat/lon) resolution, is used. It is continuously updated until present and available since the 1st of January 2011 in 6-hourly time steps. Data from the start to the 1st of January 2018 were used.

Eqs. 9–10 were used to obtain the geopotential difference between the pressure level closest to the surface and 50 hPa above this level for each grid cell, using finite-differences. A layer of 50 hPa is chosen because it is close to the mean PBL height in the mid-latitudes, $\Delta z \approx h \approx 500$ m (Peña et al., 2013). Then β was computed as

$$\beta = \arctan\left(\langle V_T \rangle_G / \Delta z, \langle U_T \rangle_G / \Delta z\right), \tag{13}$$

where the `arctan` function operates on the ratio of its second argument to the first argument, accounting for quadrants, and the angle brackets denote a conditional mean which is below. The magnitude of geostrophic shear was computed as

$$\frac{\partial |\mathbf{U}_g|}{\partial z} = \sqrt{\left(\frac{\langle U_T \rangle_G}{\Delta z}\right)^2 + \left(\frac{\langle V_T \rangle_G}{\Delta z}\right)^2}. \tag{14}$$

The WAsP stability model is developed for high wind speeds, because these are most important to determine the wind power density at a site of interest (Troen and Petersen, 1989; Kelly et al., 2014). Therefore in Eqs. 13–14 we use a conditional mean denoted by $\langle\rangle_G$, defined for each grid point as when the surface geostrophic wind G_0 was higher than the median of G_0. The surface-level geostrophic wind components

$$U_g = -\frac{1}{f}\frac{\partial \Phi_0}{\partial y}, \qquad V_g = \frac{1}{f}\frac{\partial \Phi_0}{\partial x} \tag{15}$$

are computed from the re-analysis (CFSR) data, which give the magnitude of 'surface' geostrophic wind

$$G_0 = |\mathbf{U}_{g,0}| = \sqrt{U_{g,0}^2 + V_{g,0}^2}. \tag{16}$$

Due to the large number of grid points and the large volume of data involved, an MPI implementation was developed to compute these means. Using this script, the 1764 GB of data can be processed on DTU's HPC cluster Jess using 20 processors in approximately 5 min. Because $1/f \to \infty$ approaching the equator, it was chosen to be a constant ($f = 10^{-4}\,\mathrm{s}^{-1}$). This value is the same as in the stability implementation of WAsP.

1.4 Global geostrophic wind shear

Fig. 1 shows the conditional mean geostrophic shear from 2011 to 2017. It can be seen that high geostrophic wind shears are observed near the antarctic plateau, where katabatic winds are common and geostrophic wind shear is known to be high (Mahrt and Schwerdtfeger, 1970). However, due to limited interest for wind energy applications these extreme values are of little concern. Also near mountain ranges, such as the himalayas, high values of geostropic wind shear can be observed. Such high values can potentially cause unexpected results in WAsP and therefore geostrophic wind shear is truncated beyond 0.012 s^{-1} and a warning is shown. Other areas with high geostrophic wind shear values are located near the coast or in regions with strong horizontal gradients in sea surface temperature.

1.5 Validation of WAsP12 versus WAsP 12.1

To evaluate whether the inclusion of geostrophic wind shear improves the wind modelling, we perform cross predictions at 66 sites. A cross prediction is defined as the prediction of the flow from one observed wind climate, a specific mast and height, to another observed position, either another height on the same mast or an observed height on another mast. The relative errors for each cross prediction were computed as a percentage from the observed (obs) and modelled data (mod) as $\delta = 100(mod - obs)/obs$ for both wind speed (δU) and

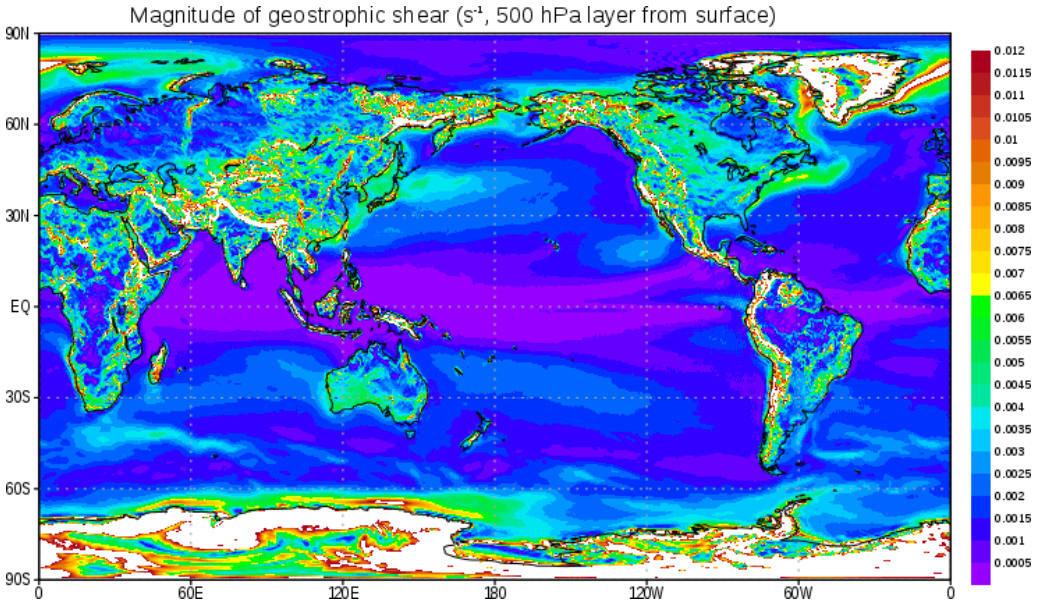

Figure 1: Magnitude of geostrophic wind shear obtained from CFSR reanalysis data, version 2 (see text). White areas show the regions where WAsP12 will truncate the contribution of geostrophic wind shear.

power density (δP). It is important to include power density in the evaluation, since the production of wind turbines is determined by the available power. The total power density is calculated by summation of the frequency weighted third moment of the Weibull distribution from each sector of the total of number of sectors D,

$$P = \sum_{l=1}^{D} 0.5 \rho f_l A_l^3 \Gamma(1 + 3/k_l), \tag{17}$$

where ρ is a reference air density (here 1.225 kg m^{-3}), f is the frequency of occurrence and k is the shape parameter of the Weibull distribution.

We only use upward cross-predictions between 40 and 200 m, because close to the ground terrain effects will contribute significantly to the observed errors. The default WAsP heat flux parameters were used. These default are a offset heatflux of -40 and -8 W m^{-2} over land and sea, respectively. The RMS heat flux is prescribed to be 100 and 30 W m^{-2} over land and sea, respectively. Furthermore, self-predictions are excluded. Finally, we compute a mean relative error δE from the mean of δU and δP, which are shown in Table 1. The validation is split up in three categories:

- All cross-predictions, which constitutes 1085 cross-predictions with 60 different masts.
- Cross-predictions in simple terrain from one height to another at the same mast (RIX=0.0), 312 cross-predictions at 19 masts.
- Horizontal, i.e. from one mast to another mast, which are important to evaluate conditions when the mesoscale roughness is largely different, 610 cross-predictions at 34 masts.

It can be observed that in all cases, WAsP12 with geostrophic wind shear turned on shows a minor but consistent improvement compared to the model which has it switched off. As expected, the largest relative errors occur when performing horizontal cross-predictions, whereas for the cross-predictions in terrain with no slopes of more than 30°(RIX=0.0) are around 2%. All cross-predictions combined are between these two with errors around 6%. Note that there is significant amount of complex and forested sites among all cross-predictions.

Model	δE all	δE, RIX=0.0	δE, horizontal
WAsP12.1, no geo. wind shear	6.54	2.36	9.00
WAsP12.1, with geo. wind shear	6.49	2.30	8.94

Table 1: *Mean relative error for (1) all cross-predictions; (2) cross-predictions over simple terrain from one height to another on the same mast; and (3) cross-predictions from one mast to another, where the roughnesses differ.*

1.6 Geostrophic wind shear in the WAsP user interface

The method discussed above is reduced to prescribing the parameters $\frac{\partial|\mathbf{U}_g|}{\partial z}$ (magnitude of geostrophic shear) and β (direction of geostrophic shear), that are automatically filled from the global CFSR data when a user creates a generalised wind climate (GWC). Based on the location of the observed wind climate, the nearest grid point from the CFSR data is chosen and the two parameters are extracted and shown to the user (Fig. 2). By default it will be turned on, but it can be switched off by ticking the box next to "Use geostrophic shear" (see Fig. 2), which will highlight the option in yellow. The result without geostrophic wind shear switched on will be nearly identical to WAsP 12 and previous versions.

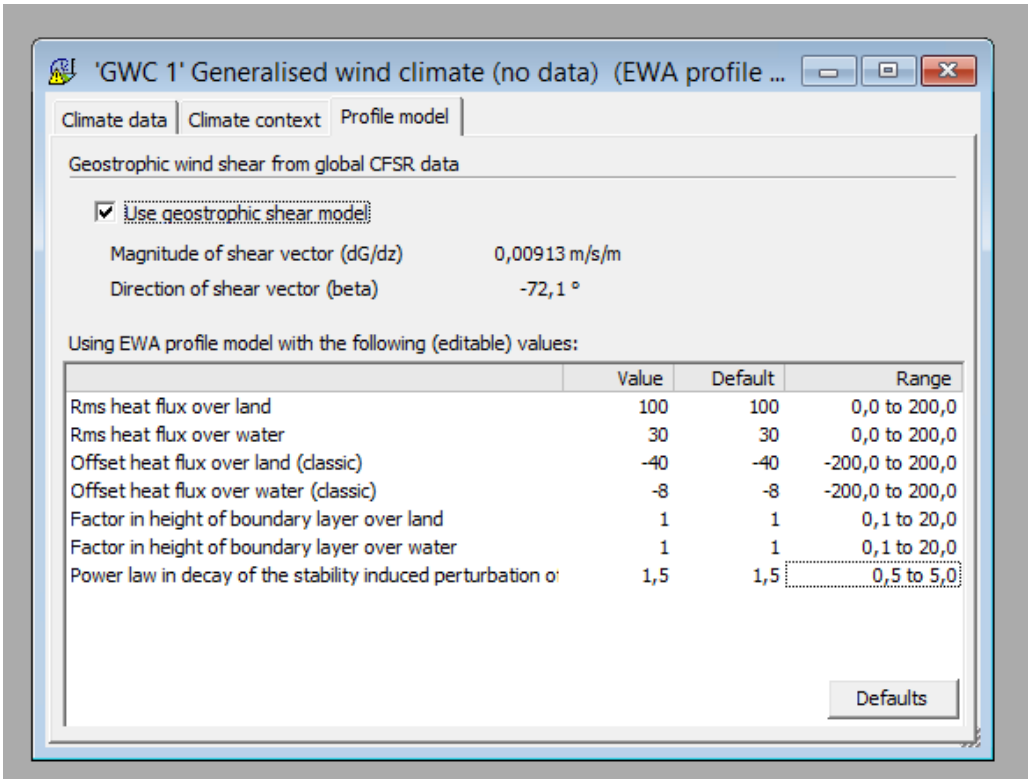

Figure 2: Specifying the geostrophic wind shear in the WAsP user interface in the profile model.

2 Conclusion

A new version of WAsP, 12.1, has been developed. This version includes modelling of average geostrophic wind shear (baroclinicity), which is obtained from a global reanalysis data set from the CFSR data set. Using 60 different masts at a variety of sites (both simple and complex terrain) throughout the world showed that the model slightly improved the model

skills expressed in terms of weighted wind speed and power density errors.

References

Arya, S. P. S. (1978). Comparative Effects of Stability, Baroclinity and the Scale-Height Ratio on Drag Laws for the Atmospheric Boundary Layer. *J. Atmos. Sci.*, 35(1):40–46.

Arya, S. P. S. and Wyngaard, J. C. (1975). Effect of Baroclinicity on Wind Profiles and the Geostrophic Drag Law for the Convective Planetary Boundary Layer. *J. Atmos. Sci.*, 32(4):767–778.

Blackadar, A. K. and Tennekes, H. (1968). Asymptotic Similarity in Neutral Barotropic Planetary Boundary Layers. *J. Atmos. Sci.*, 25(6):1015–1020.

Businger, J. A., Wyngaard, J. C., Izumi, Y., and Bradley, E. F. (1971). Flux-Profile Relationships in the Atmospheric Surface Layer. *J. Atmos. Sci.*, 28(2):181–189.

Floors, R., Peña, A., and Gryning, S.-E. (2015). The effect of baroclinicity on the wind in the planetary boundary layer. *Q. J. R. Meteorol. Soc.*, 141(687):619–630.

Hess, G. D. and Garratt, J. R. (2002). Evaluating Models of The Neutral, Barotropic Planetary Boundary Layer using Integral Measures: Part I. Overview. *Boundary-Layer Meteorol.*, 104(3):333–358.

Holton, J. R. and Hakim, G. J. (2004). *An introduction to dynamic meteorology*. Elsevier Academic press, 4th edition.

Jensen, N. O. (1978). Change of surface roughness and the planetary boundary layer. *Q. J. R. Meteorol. Soc.*, 104(440):351–356.

Kelly, M. and Troen, I. (2016). Probabilistic stability and 'tall' wind profiles: theory and method for use in wind resource assessment. *Wind Energy*, 19(2):227–241.

Kelly, M., Troen, I., and Jørgensen, H. E. (2014). Weibull-k Revisited: "Tall" Profiles and Height Variation of Wind Statistics. *Boundary-Layer Meteorol.*, 152(1):107–124.

Mahrt, L. J. and Schwerdtfeger, W. (1970). Ekman spirals for exponential thermal wind. *Boundary-Layer Meteorol.*, 1(2):137–145.

Peña, A., Gryning, S.-E., and Hahmann, A. (2013). Observations of the atmospheric boundary layer height under marine upstream flow conditions at a coastal site. *J. Geophys. Res. Atmos.*, 118(4):1924–1940.

Saha, S., Moorthi, S., Wu, X., Wang, J., Nadiga, S., Tripp, P., Behringer, D., Hou, Y.-T., Chuang, H.-y., Iredell, M., Ek, M., Meng, J., Yang, R., Mendez, M. P., van den Dool, H., Zhang, Q., Wang, W., Chen, M., and Becker, E. (2014). The NCEP Climate Forecast System Version 2. *J. Clim.*, 27(6):2185–2208.

Troen, I. and Petersen, E. L. (1989). *European Wind Atlas*. Risø National Laboratory, Roskilde, Denmark.

DTU Wind Energy is a department of the Technical University of Denmark with a unique integration of research, education, innovation and public/private sector consulting in the field of wind energy. Our activities develop new opportunities and technology for the global and Danish exploitation of wind energy. Research focuses on key technical-scientific fields, which are central for the development, innovation and use of wind energy and provides the basis for advanced education at the education.

We have more than 240 staff members of which approximately 60 are PhD students. Research is conducted within nine research programmes organized into three main topics: Wind energy systems, Wind turbine technology and Basics for wind energy.

Technical University of Denmark
Department of Wind Energy
Frederiksborgvej 399
Building 118
4000 Roskilde
Denmark
Telephone 46 77 50 85

info@vindenergi.dtu.dk
www.vindenergi.dtu.dk